Structural Engineering and Mechanics, *Vol. 64, No. 4 (2017) 515-526*
DOI: https://doi.org/10.12989/sem.2017.64.4.515

Moving load induced dynamic response of functionally graded-carbon nanotubes-reinforced pipes conveying fluid subjected to thermal load

F. Vakili Tahami*, H. Biglari and M. Raminnea

Faculty of Mechanical Engineering, University of Tabriz, Tabriz, Iran

(Received June 19, 2017, Revised August 19, 2017, Accepted September 12, 2017)

Abstract. Dynamic response of functionally graded Carbon nanotubes (FG-CNT) reinforced pipes conveying viscous fluid under accelerated moving load is presented. The mixture rule is used for obtaining the material properties of nano-composite pipe. The radial force induced by viscous fluid is calculated by Navier–Stokes equation. The material properties of pipe are considered temperature-dependent. The structure is simulated by Reddy higher-order shear deformation shell theory and the corresponding motion equations are derived by Hamilton's principal. Differential quadrature (DQ) method and the Integral Quadrature (IQ) are applied for analogizing the motion equations and then the Newmark time integration scheme is used for obtaining the dynamic response of structure. The effects of different parameters such as boundary conditions, geometrical parameters, velocity and acceleration of moving load, CNT volume percent and distribution type are shown on the dynamic response of pipe. Results indicate that increasing CNTs leads to decrease in transient deflection of structure. In accelerated motion of the moving load, the maximum displacement is occurred later with respect to decelerated motion of moving load.

Keywords: dynamic response; FG-CNT pipe; moving load; viscous fluid; DQ-IQ method

1. Introduction

In structural dynamics, the importance of moving load problem is very significant. Vehicles that pass bridges, trains on the track, guideways, roadways, runways of airports with aircrafts, piping systems are examples of this problem. In the mentioned structures, the main emphasis is placed on obtaining the dynamic displacements caused by the moving loads. However, the accurate calculation of the dynamic response of structures subjected to moving load is essential for design and life prediction of them. On the other hand, nanotechnology is a new subject in the word which is taken into consideration by many researchers. Hence, in the present work, dynamic response of a nano-composite pipe conveying fluid subjected to accelerated moving load is studied.

Dynamic responses of a flat plate subjected to various moving loads were studied by We *et al*. (1987) using finite element method. The dynamic behaviour of a saggy suspension cable under a moving load was investigated by Wu and Chen (1989). A theoretical analysis of the axially-symmetric, steady-state response of a linearly-elastic, homogeneous, infinitely-long, cylindrical shell, subjected to a ring load traveling at a constant velocity was presented by Huang (1976). Chonan (1981) studied the response to a moving ring load of an infinitely long two layered cylindrical shell with a flexible bond at the interface. Sheng (1985) discussed the forced vibrations of the elastic shallow shell due to the moving mass by means of the variational method. A theoretical model was developed by Panneton *et al*. (1995) to evaluate the vibration and sound radiation of a thin cylindrical shell excited by a constant point load continuously traveling along the circumferential direction at a rotational speed. Sing *et al*. (1999) investigated Non-axisymmetric dynamic response of buried orthotropic cylindrical shells under moving load. An accurate and effective solution for a circular curved beam subjected to a moving load was proposed by Huang *et al*. (2000), which incorporates the dynamic stiffness matrix into the Laplace transform technique. The dynamic behavior of an orthotropic plate simply supported on a pair of parallel edges and under a system of moving loads was analyzed by Zhu and Law (2003) based on Lagrange equation and modal superposition. A finite element model (FEM) was developed by Ruzzene and Bazto (2006) analyze the dynamic response of axi-symmetric shells subjected to axially moving loads. A method was proposed by Bespalova (2007) to determine the stress-strain state of inhomogeneous anisotropic viscoelastic cylindrical shells subject to a load moving along the circumference with a given velocity. Different aspects of dynamic identification of moving loads from a vehicle traveling on top of a beam-slab type bridge deck were studied by Law *et al*. (2007). The bridge deck was modeled as an orthotropic plate and the loads were modeled as a group of wheel loads or a group of axle loads moving on top of the bridge deck at a fixed spacing. Yang *et al*. (2008) presented an analytical study on the free and forced vibration of inhomogeneous Euler–Bernoulli beams containing open edge cracks. The beam was subjected to an axial compressive force and a concentrated transverse load moving along the longitudinal direction. Based on the first-order shear deformation theory (FSDT), the Hamilton's principle and the Maxwell

*Corresponding author, Ph.D.
E-mail: f_vakili@tabrizu.ac.ir

ISSN: 1225-4568 (Print), 1598-6217 (Online)

equation, Sheng and Wang (2009) presented the coupling equations to govern the electric potential and the displacements of the functionally graded cylindrical shell with surface-bonded PZT piezoelectric layer, and subjected to moving loads. In another work by the same authors (2010), an approximate solution for FG laminated piezoelectric cylindrical shells under thermal shock and moving mechanical loads was given utilizing Hamilton's principle. The dynamic response of angle-ply laminated composite plates traversed by a moving mass or a moving force was investigated by Ghafoori and Asghari (2010). Sofiyev (2010) presented an analytical study on the dynamic behavior of the infinitely-long, FGM cylindrical shell subjected to combined action of the axial tension, internal compressive load and ring-shaped compressive pressure with constant velocity. Sadeghi and Karimi-Dona (2011) studied the dynamic behavior of a pipe conveying fluid, with a sprung mass moving on it using the Galerkin method with appropriate shape functions.

The dynamic responses of an elastic rectangular plate to some types of moving loads' distribution were obtained and compared by Gbadeyan and Dada (2011). Eftekhari and Jafari (2012) presented a combined application of the Ritz method, the DQ method, and the IQ method to vibration problem of rectangular plates subjected to accelerated traveling masses. The propagation of steady-state vibration in a periodic pipe conveying fluid on elastic foundation with an external moving load was studied by Yu *et al*. (2012) using wave propagation and attenuation theory. The transient thermo-elastic analysis of FG cylindrical shells, FG plates and FG truncated conical shells under moving load was presented by Malekzadeh and co-authors (2012; 2013 and 2014). Wave propagation in sandwich structures with periodic assemblies on elastic foundation under external moving load was studied by Chen and Tsai (2014). Dynamic behaviour of simply supported uniform beams subjected to a single moving point load was analyzed by Kumar *et al*. (2015). Castro Jorge *et al*. (2015) presented a study on the dynamic response of beams on nonlinear elastic foundations, subjected to moving loads. He and Zhu (2015) investigated the closed-form solution of the dynamic response of a damaged simply supported beam subjected to a moving load and examined the effects of the loss of local stiffness on these two components. Attar *et al*. (2015) presented a semi-analytical approach to predict the forced response of a multi-cracked Timoshenko beam traversed by a moving harmonic load with constant speed. Eftekhari (2016) demonstrated the in-plane vibration analysis of variable thickness circular arches traversed by a moving point load using DQM. The propagation and attenuation properties of waves in ordered and disordered periodic composite Timoshenko beams, which consider the effects of axial static load and structural damping, resting on elastic foundations were studied by Ding *et al*. (2016) when the system is subjected to moving loads of constant amplitude with a constant velocity. A moving bounds strategy was proposed by Wang *et al*. (2016) to implement simultaneous shape optimization of curved shell structures and openings. A comprehensive method was proposed by Song *et al*. (2016) to predict the dynamic behaviors of flat plate of arbitrary boundary conditions subjected to moving loads, based on Kirchhoff plate theory. Kaur *et al*. (2016) studied the stress produced in an irregular fiber-reinforced half-space due to a normal moving load on a free surface. Dynamic response of an axially functionally graded (AFG) beam under thermal environment subjected to a moving harmonic load was investigated by Wang and Wu (2016) within the frameworks of classical beam theory and Timoshenko beam theory.

As reported above, there are many works for the dynamic analysis of beam/plate/shell subjected to moving load. However, to the best of the author's knowledge, in spite of its importance, no research work related to the dynamic response of FG-CNT-reinforced pipes conveying fluid under moving loads has been yet presented. The main novelties of this work are considering combination of pipe reinforced by FG-CNT, temperature-dependent material properties of pipe, viscous fluid flow in the pipe, accelerated moving load, Reddy shear deformation theory for modeling and utilizing three numerical method for solution. The rule of mixture and Navier–Stokes equation are used for obtaining the equivalent material properties of structure and radial force induced by fluid, respectively. Applying energy method and Hamilton's principal, the nonlinear motion equations are derived for Reddy pipe. DQ-IQ methods in conjunction with Newmark time integration scheme are utilized for calculating the transient displacement of system. The effects of the CNTs distribution type, geometrical parameters, volume fractions of CNTs, boundary conditions and moving load velocity and acceleration on the dynamic response of the FG-CNT pipe are investigated.

2. Basic theories

2.1 Mixture rule

In order to obtain the equivalent material properties two phase nano-composites (i.e., polymer as matrix and CNT as reinforcer), the rule of mixture (Liew *et al*. 2014) is applied. According to mixture rule, the effective Young and shear moduli of nano-composite structure can be written as

$$E_{11} = \eta_1 V_{CNT} E_{r11} + (1 - V_{CNT}) E_m, \tag{1}$$

$$\frac{\eta_2}{E_{22}} = \frac{V_{CNT}}{E_{r22}} + \frac{(1 - V_{CNT})}{E_m}, \tag{2}$$

$$\frac{\eta_3}{G_{12}} = \frac{V_{CNT}}{G_{r12}} + \frac{(1 - V_{CNT})}{G_m}, \tag{3}$$

where E_{r11}, E_{r22} and G_{r11} indicate the Young's moduli and shear modulus of CNTs, respectively, and E_m, G_m represent the corresponding properties of the isotropic matrix. With the knowledge that load transfer between the nanotube and polymeric phases is less than perfect (e.g., the surface effects, strain gradients effects, intermolecular coupled stress effects, etc.), we introduced η_j (j=1, 2, 3) into Eqs. (3)-(3) to consider the size-dependent material properties. η_j

is called the CNT efficiency parameter which will be determined later by matching the elastic modulus of system observed from the molecular dynamic (MD) simulation results with the numerical results obtained from the rule of mixture. V_{CNT} and V_m are the volume fractions of the CNTs and matrix, respectively, which the sum of them equals to unity. The uniform and three types of FG distributions of the CNTs along the thickness direction of the nano-composite structure take the following forms (Liew *et al.* 2014)

$$UD:\ V_{CNT}=V_{CNT}^{*}, \tag{4}$$

$$FGV:\ V_{CNT}(z)=\left(1-\frac{2z}{h}\right)V_{CNT}^{*}, \tag{5}$$

$$FGO:\ V_{CNT}(z)=2\left(1-\frac{2|z|}{h}\right)V_{CNT}^{*}, \tag{6}$$

$$FGX:\ V_{CNT}(z)=2\left(\frac{2|z|}{h}\right)V_{CNT}^{*}, \tag{7}$$

where

$$V_{CNT}^{*}=\frac{w_{CNT}}{w_{CNT}+(\rho_{CNT}/\rho_m)-(\rho_{CNT}/\rho_m)w_{CNT}}, \tag{8}$$

where w_{CNT}, ρ_m and ρ_{CNT} are the mass fraction of the SWCNT, the densities of the matrix and SWCNT, respectively. Similarly, the thermal expansion coefficients in the longitudinal and transverse directions respectively (α_{11} and α_{22}), and the density (ρ) of the CNTRC pipes can be determined as

$$\rho=V_{CNT}^{*}\rho_r+V_{m,}\rho_{m,}, \tag{9}$$

$$\alpha_{11}=V_{CNT}^{*}\alpha_{r11}+V_{m,}\alpha_{m,}, \tag{10}$$

$$\alpha_{22}=(1+\nu_{r12})V_{CNT}\alpha_{r22}+(1+\nu_m)V_m\alpha_m-\nu_{12}\alpha_{11}, \tag{11}$$

where α_{r11}, α_{r22} and α_m are the thermal expansion coefficients of the CNT and matrix, respectively. It should be noted that ν_{12} is assumed as constant over the thickness of the structure.

2.2 Reddy higher order shear deformation theory

Based on Reddy shell theory, the displacement field can be expressed as (Reddy 1984)

$$u_x(x,\theta,z,t)=u\ (x,\theta,t)+z\,\psi_x(x,\theta,t)-\frac{4z^3}{3h^2}\left(\psi_x(x,\theta,t)+\frac{\partial}{\partial x}w\ (x,\theta,t)\right), \tag{12}$$

$$u_\theta(x,\theta,z,t)=v\,(x,\theta,t)+z\,\psi_\theta(x,\theta,t)-\frac{4z^3}{3h^2}\left(\psi_\theta(x,\theta,t)+\frac{\partial}{R\partial\theta}w\ (x,\theta,t)\right), \tag{13}$$

$$u_z(x,\theta,z,t)=w(x,\theta,t), \tag{14}$$

where (u_x, u_θ, u_z) denote the displacement components at an arbitrary point (x,θ,z) in the pipe, and (u,v,w) are the displacement of a material point at (x, θ) on the mid-plane (i.e., z=0) of the pipe along the x-, θ-, and z-directions, respectively; ψ_x and ψ_θ are the rotations of the normal to the mid-plane about θ- and x- directions, respectively. The von Kármán strains associated with the above displacement field can be expressed in the following form

$$\begin{Bmatrix}\varepsilon_{xx}\\ \varepsilon_{\theta\theta}\\ \varepsilon_{x\theta}\\ \varepsilon_{xz}\\ \varepsilon_{\theta z}\end{Bmatrix}=\begin{Bmatrix}\varepsilon_{xx}^{0}\\ \varepsilon_{\theta\theta}^{0}\\ \varepsilon_{x\theta}^{0}\\ \varepsilon_{xz}^{0}\\ \varepsilon_{\theta z}^{0}\end{Bmatrix}+z\begin{Bmatrix}\varepsilon_{xx}^{1}\\ \varepsilon_{\theta\theta}^{1}\\ \varepsilon_{x\theta}^{1}\\ \varepsilon_{xz}^{1}\\ \varepsilon_{\theta z}^{1}\end{Bmatrix}+z^2\begin{Bmatrix}\varepsilon_{xx}^{2}\\ \varepsilon_{\theta\theta}^{2}\\ \varepsilon_{x\theta}^{2}\\ \varepsilon_{xz}^{2}\\ \varepsilon_{\theta z}^{2}\end{Bmatrix}+z^3\begin{Bmatrix}\varepsilon_{xx}^{3}\\ \varepsilon_{\theta\theta}^{3}\\ \varepsilon_{x\theta}^{3}\\ \varepsilon_{xz}^{3}\\ \varepsilon_{\theta z}^{3}\end{Bmatrix}, \tag{15}$$

where

$$\begin{Bmatrix}\varepsilon_{xx}^{0}\\ \varepsilon_{\theta\theta}^{0}\\ \varepsilon_{x\theta}^{0}\\ \varepsilon_{xz}^{0}\\ \varepsilon_{\theta z}^{0}\end{Bmatrix}=\begin{Bmatrix}\dfrac{\partial u}{\partial x}+\dfrac{1}{2}\left(\dfrac{\partial w}{\partial x}\right)^2\\ \dfrac{\partial v}{R\partial\theta}+\dfrac{w}{R}+\dfrac{1}{2}\left(\dfrac{\partial w}{R\partial\theta}\right)^2\\ \dfrac{\partial v}{\partial x}+\dfrac{\partial u}{R\partial\theta}+\dfrac{\partial w}{\partial x}\dfrac{\partial w}{R\partial\theta}\\ \psi_x+\dfrac{\partial w}{\partial x}\\ \psi_\theta+\dfrac{\partial w}{R\partial\theta}\end{Bmatrix}, \tag{16}$$

$$\begin{Bmatrix}\varepsilon_{xx}^{1}\\ \varepsilon_{\theta\theta}^{1}\\ \varepsilon_{x\theta}^{1}\\ \varepsilon_{xz}^{1}\\ \varepsilon_{\theta z}^{1}\end{Bmatrix}=\begin{Bmatrix}\dfrac{\partial\psi_x}{\partial x}\\ \dfrac{\partial\psi_\theta}{R\partial\theta}\\ \dfrac{\partial\psi_x}{R\partial\theta}+\dfrac{\partial\psi_\theta}{\partial x}\\ 0\\ 0\end{Bmatrix}, \tag{17}$$

$$\begin{Bmatrix}\varepsilon_{xx}^{2}\\ \varepsilon_{\theta\theta}^{2}\\ \varepsilon_{x\theta}^{2}\\ \varepsilon_{xz}^{2}\\ \varepsilon_{\theta z}^{2}\end{Bmatrix}=\begin{Bmatrix}0\\ 0\\ 0\\ \dfrac{-4}{h^2}\left(\psi_x+\dfrac{\partial w}{\partial x}\right)\\ \dfrac{-4}{h^2}\left(\psi_\theta+\dfrac{\partial w}{R\partial\theta}\right)\end{Bmatrix}, \tag{18}$$

$$\begin{Bmatrix}\varepsilon_{xx}^{3}\\ \varepsilon_{\theta\theta}^{3}\\ \varepsilon_{x\theta}^{3}\\ \varepsilon_{xz}^{3}\\ \varepsilon_{\theta z}^{3}\end{Bmatrix}=\begin{Bmatrix}\dfrac{-4}{3h^2}\left(\dfrac{\partial\psi_x}{\partial x}+\dfrac{\partial^2 w}{\partial x^2}\right)\\ \dfrac{-4}{3h^2}\left(\dfrac{\partial\psi_\theta}{R\partial\theta}+\dfrac{\partial^2 w}{R^2\partial\theta^2}\right)\\ \dfrac{-4}{3h^2}\left(\dfrac{\partial\psi_\theta}{\partial x}+\dfrac{\partial\psi_x}{R\partial\theta}+2\dfrac{\partial^2 w}{R\partial x\partial\theta}\right)\\ 0\\ 0\end{Bmatrix}, \tag{19}$$

where (ε_{xx}, $\varepsilon_{\theta\theta}$) are the normal strain components and ($\gamma_{\theta x}$, γ_{xz}, $\gamma_{x\theta}$) are the shear strain components.

2.3 Stress-strain relations

The constitutive equation for stresses $\boldsymbol{\sigma}$ and strains $\boldsymbol{\varepsilon}$ matrix in thermal environment may be written as follows

$$\begin{Bmatrix}\sigma_{xx}\\ \sigma_{\theta\theta}\\ \sigma_{\theta z}\\ \sigma_{zx}\\ \sigma_{x\theta}\end{Bmatrix}=\begin{bmatrix}C_{11}(z,T) & C_{12}(z,T) & 0 & 0 & 0\\ C_{21}(z,T) & C_{22}(z,T) & 0 & 0 & 0\\ 0 & 0 & C_{44}(z,T) & 0 & 0\\ 0 & 0 & 0 & C_{55}(z,T) & 0\\ 0 & 0 & 0 & 0 & C_{66}(z,T)\end{bmatrix}\begin{Bmatrix}\varepsilon_{xx}-\alpha_{xx}\Delta T\\ \varepsilon_{\theta\theta}-\alpha_{\theta\theta}\Delta T\\ \gamma_{\theta z}\\ \gamma_{xz}\\ \gamma_{x\theta}\end{Bmatrix}, \tag{20}$$

Noted that C_{ij} and α_{xx}, $\alpha_{\theta\theta}$ may be obtained using Eqs. (1)-(3).

3. Mathematical modeling of structure

As shown in Fig. 1, a FG-CNT reinforced pipe conveying viscous fluid under a moving load with length L and thickness h is considered. Four types of CNT distribution namely as uniform distribution (UD) along with FG distributions (FGA, FGO, FGX) along the thickness direction pipe are considered. Here, the energy method and Hamilton's principal are used for obtaining the motion equations.

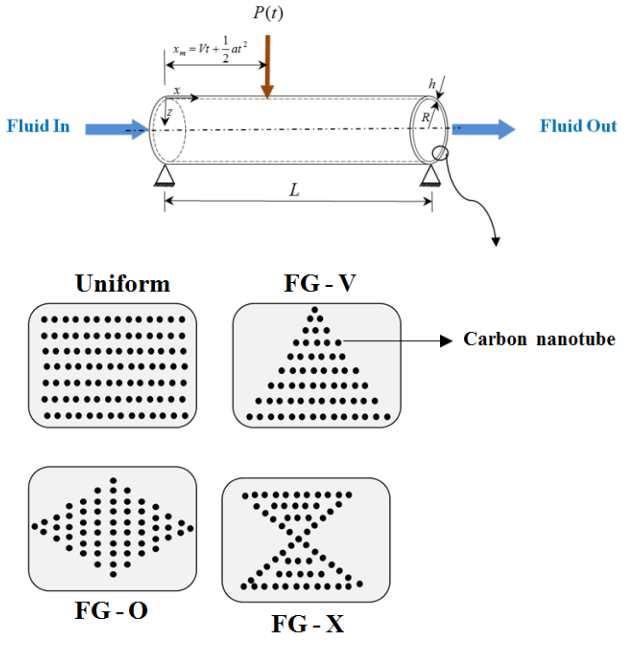

Fig. 1 Schematic of the FG-CNT-reinforced pipe conveying fluid under moving load

3.1 Energy method

The strain energy can be written as

$$U=\frac{1}{2}\int_{\Omega_0}\int_{-h/2}^{h/2}\begin{pmatrix}\sigma_{xx}\varepsilon_{xx}+\sigma_{\theta\theta}\varepsilon_{\theta\theta}+\sigma_{x\theta}\gamma_{x\theta}\\ +\sigma_{xz}\gamma_{xz}+\sigma_{\theta z}\gamma_{\theta z}\end{pmatrix}dV\ , \tag{21}$$

Combining of Eqs. (15)-(19) and (21) yields

$$\begin{aligned}U=&\frac{1}{2}\int_{\Omega_0}\left(N_{xx}\left(\frac{\partial u}{\partial x}+\frac{1}{2}\left(\frac{\partial w}{\partial x}\right)^2\right)+N_{\theta\theta}\left(\frac{\partial v}{\partial\theta}+\frac{w}{R}+\frac{1}{2}\left(\frac{\partial w}{R\partial\theta}\right)^2\right)\right.\\&+Q_\theta\left(\frac{\partial w}{R\partial\theta}+\psi_\theta\right)+Q_x\left(\frac{\partial w}{\partial x}+\psi_x\right)+N_{x\theta}\left(\frac{\partial v}{\partial x}+\frac{\partial u}{R\partial\theta}+\frac{\partial w}{\partial x}\frac{\partial w}{R\partial\theta}\right)\\&+M_{xx}\frac{\partial\psi_x}{\partial x}+M_{\theta\theta}\frac{\partial\psi_\theta}{R\partial\theta}+M_{x\theta}\left(\frac{\partial\psi_x}{R\partial\theta}+\frac{\partial\psi_\theta}{\partial x}\right)+K_\theta\left(\frac{-4}{h^2}\left(\psi_\theta+\frac{\partial w}{R\partial\theta}\right)\right)\\&+K_x\left(\frac{-4}{h^2}\left(\psi_x+\frac{\partial w}{\partial x}\right)\right)+P_{xx}\left(\frac{-4}{3h^2}\left(\frac{\partial\psi_x}{\partial x}+\frac{\partial^2 w}{\partial x^2}\right)\right)\\&\left.+P_{\theta\theta}\left(\frac{-4}{3h^2}\left(\frac{\partial\psi_\theta}{R\partial\theta}+\frac{\partial^2 w}{R^2\partial\theta^2}\right)\right)+P_{x\theta}\left(\frac{\partial\psi_\theta}{\partial x}+\frac{\partial\psi_x}{R\partial\theta}+2\frac{\partial^2 w}{R\partial x\,\partial\theta}\right)\right)dx\,d\theta,\end{aligned} \tag{22}$$

where the stress resultant-displacement relations can be written as

$$\left(\begin{Bmatrix}N_{xx}\\ N_{\theta\theta}\\ N_{x\theta}\end{Bmatrix},\begin{Bmatrix}M_{xx}\\ M_{\theta\theta}\\ M_{x\theta}\end{Bmatrix},\begin{Bmatrix}P_{xx}\\ P_{\theta\theta}\\ P_{x\theta}\end{Bmatrix}\right)=\int_{-h/2}^{h/2}\begin{bmatrix}\sigma_{xx}\\ \sigma_{\theta\theta}\\ \sigma_{x\theta}\end{bmatrix}(1,z,z^3)dz, \tag{23}$$

$$\left(\begin{Bmatrix}Q_x\\ Q_\theta\end{Bmatrix},\begin{Bmatrix}K_x\\ K_\theta\end{Bmatrix}\right)=\int_{-h/2}^{h/2}\begin{bmatrix}\sigma_{xz}\\ \sigma_{\theta z}\end{bmatrix}(1,z^2)dz, \tag{24}$$

The kinetic energy of system may be written as

$$K=\frac{\rho}{2}\int_{\Omega_0}\int_{-h/2}^{h/2}\left((\dot{u}_x)^2+(\dot{u}_\theta)^2+(\dot{u}_z)^2\right)dV\ , \tag{25}$$

The external work is divided into two parts of fluid and moving load. However, we have

$$W=\int_0^L\left(P_{Fluid}+P_{Load}\right)w\,dA, \tag{26}$$

where the force induced by fluid and moving load can be written as (Raminnea *et al*. 2016, Kolahchi *et al*. 2016a)

$$\begin{aligned}P_{fluid}=&h_f\frac{\partial p_z}{\partial z}=-\rho_f h_f\left(\frac{\partial^2 w}{\partial t^2}+2v_x\frac{\partial^2 w}{\partial x\,\partial t}+v_x{}^2\frac{\partial^2 w}{\partial x^2}\right)\\&+\mu h_f\left(\frac{\partial^3 w}{\partial x^2\partial t}+\frac{\partial^3 w}{R^2\partial\theta^2\partial t}+v_x\left(\frac{\partial^3 w}{\partial x^3}+\frac{\partial^3 w}{R^2\partial\theta^2\partial x}\right)\right),\end{aligned} \tag{27}$$

$$P_{load}=F_0\delta(x-x_m), \tag{28}$$

where μ, v_x and ρ_f are respectively, viscosity, mean flow velocity and density of fluid; F_0 is the amplitude of the moving load; $\delta(x)$ is the Dirac delta-function; x_m is the position co-ordinate of the moving load in x-direction which can be defined as

$$x_m=Vt+\frac{1}{2}at^2, \tag{29}$$

where V and a are the initial velocity and acceleration of the moving load, respectively.

3.2 Motion equations

The governing equations can be derived by Hamilton's principal as follows

$$\delta u: \frac{\partial N_{xx}}{\partial x}+\frac{\partial N_{x\theta}}{R\partial\theta}=I_0\frac{\partial^2 u}{\partial t^2}+J_1\frac{\partial^2\psi_x}{\partial t^2}-\frac{4I_3}{h^2}\frac{\partial^3 w}{\partial t^2\partial x}, \tag{30}$$

$$\delta v: \frac{\partial N_{x\theta}}{\partial x}+\frac{\partial N_{\theta\theta}}{R\partial\theta}=I_0\frac{\partial^2 v}{\partial t^2}+J_1\frac{\partial^2\psi_\theta}{\partial t^2}-\frac{4I_3}{h^2}\frac{\partial^3 w}{R\partial t^2\partial\theta}, \tag{31}$$

$$\begin{aligned}&\delta w: \frac{\partial Q_x}{\partial x}+\frac{\partial Q_\theta}{R\partial\theta}-\frac{4}{h^2}\left(\frac{\partial K_x}{\partial x}+\frac{\partial K_\theta}{R\partial\theta}\right)\\&+\frac{\partial}{\partial x}\left(N_{xx}\frac{\partial w}{\partial x}+N_{x\theta}\frac{\partial w}{R\partial\theta}\right)+\frac{\partial}{R\partial\theta}\left(N_{x\theta}\frac{\partial w}{\partial x}+N_{\theta\theta}\frac{\partial w}{R\partial\theta}\right)\\&+\frac{4}{3h^2}\left(\frac{\partial^2 P_{xx}}{\partial x^2}+2\frac{\partial^2 P_{x\theta}}{R\partial x\partial\theta}+\frac{\partial^2 P_{\theta\theta}}{R^2\partial\theta^2}\right)-\frac{N_{\theta\theta}}{R}+P_{Fluid}+P_{load}=\\&I_0\frac{\partial^2 w}{\partial t^2}-\left(\frac{4}{3h^2}\right)^2 I_6\left(\frac{\partial^4 w}{\partial x^2\partial t^2}+\frac{\partial^4 w}{R^2\partial\theta^2\partial t^2}\right)\\&+\frac{4}{3h^2}\left(I_3\frac{\partial^3 u}{\partial t^2\partial x}+I_3\frac{\partial^3 v}{R\partial t^2\partial\theta}+J_4\left(\frac{\partial^3\psi_x}{\partial t^2\partial x}+\frac{\partial^3\psi_\theta}{R\partial t^2\partial\theta}\right)\right),\end{aligned} \tag{32}$$

$$\begin{aligned}&\delta\psi_x: \frac{\partial M_{xx}}{\partial x}+\frac{\partial M_{x\theta}}{R\partial\theta}-\frac{4}{3h^2}\left(\frac{\partial P_{xx}}{\partial x}+\frac{\partial P_{x\theta}}{R\partial\theta}\right)\\&-Q_x+\frac{4}{h^2}K_x=J_1\frac{\partial^2 u}{\partial t^2}+K_2\frac{\partial^2\psi_x}{\partial t^2}-\frac{4}{3h^2}J_4\frac{\partial^3 w}{\partial t^2\partial x},\end{aligned} \tag{33}$$

$$\begin{aligned}&\delta\psi_\theta: \frac{\partial M_{x\theta}}{\partial x}+\frac{\partial M_{\theta\theta}}{R\partial\theta}-\frac{4}{3h^2}\left(\frac{\partial P_{x\theta}}{\partial x}+\frac{\partial P_{\theta\theta}}{R\partial\theta}\right)\\&-Q_\theta+\frac{4}{h^2}K_\theta=J_1\frac{\partial^2 v}{\partial t^2}+K_2\frac{\partial^2\psi_\theta}{\partial t^2}-\frac{4}{3h^2}J_4\frac{\partial^3 w}{R\partial t^2\partial\theta},\end{aligned} \tag{34}$$

where

$$I_i=\int_{-h/2}^{h/2}\rho z^i dz \qquad (i=0,1,...,6), \tag{35}$$

$$J_i=I_i-\frac{4}{3h^2}I_{i+2} \qquad (i=1,4), \tag{36}$$

$$K_2=I_2-\frac{8}{3h^2}I_4+\left(\frac{4}{3h^2}\right)^2 I_6, \tag{37}$$

Substituting Eqs. (15)-(20) into Eqs. (23) and (24), the stress resultant-displacement relations can be obtained as follow

$$\begin{aligned}&N_{xx}=A_{11}\left(\frac{\partial u}{\partial x}+\frac{1}{2}\left(\frac{\partial w}{\partial x}\right)^2\right)+A_{12}\left(\frac{\partial v}{R\partial\theta}+\frac{w}{R}+\frac{1}{2}\left(\frac{\partial w}{R\partial\theta}\right)^2\right)\\&+B_{11}\left(\frac{\partial\psi_x}{\partial x}\right)+B_{12}\left(\frac{\partial\psi_\theta}{R\partial\theta}\right)+E_{11}\left(\frac{-4}{3h^2}\left(\frac{\partial\psi_x}{\partial x}+\frac{\partial^2 w}{\partial x^2}\right)\right)\\&+E_{12}\left(\frac{-4}{3h^2}\left(\frac{\partial\psi_\theta}{R\partial\theta}+\frac{\partial^2 w}{R^2\partial\theta^2}\right)\right)-N_{xx}^T,\\&N_{\theta\theta}=A_{12}\left(\frac{\partial u}{\partial x}+\frac{1}{2}\left(\frac{\partial w}{\partial x}\right)^2\right)+A_{22}\left(\frac{\partial v}{R\partial\theta}+\frac{w}{R}+\frac{1}{2}\left(\frac{\partial w}{R\partial\theta}\right)^2\right)\\&+B_{12}\left(\frac{\partial\psi_x}{\partial x}\right)+B_{22}\left(\frac{\partial\psi_\theta}{R\partial\theta}\right)+E_{12}\left(\frac{-4}{3h^2}\left(\frac{\partial\psi_x}{\partial x}+\frac{\partial^2 w}{\partial x^2}\right)\right)\\&+E_{22}\left(\frac{-4}{3h^2}\left(\frac{\partial\psi_\theta}{R\partial\theta}+\frac{\partial^2 w}{R^2\partial\theta^2}\right)\right)-N_{\theta\theta}^T,\\&N_{x\theta}=A_{66}\left(\frac{\partial u}{R\partial\theta}+\frac{\partial v}{\partial x}+\frac{\partial w}{\partial x}\frac{\partial w}{R\partial\theta}\right)+B_{66}\left(\frac{\partial\psi_x}{R\partial\theta}+\frac{\partial\psi_\theta}{\partial x}\right)\\&+E_{66}\left(\frac{-4}{3h^2}\left(\frac{\partial\psi_\theta}{\partial x}+\frac{\partial\psi_x}{R\partial\theta}+2\frac{\partial^2 w}{R\partial x\partial\theta}\right)\right),\end{aligned} \tag{38}$$

$$\begin{aligned}&M_{xx}=B_{11}\left(\frac{\partial u}{\partial x}+\frac{1}{2}\left(\frac{\partial w}{\partial x}\right)^2\right)+B_{12}\left(\frac{\partial v}{R\partial\theta}+\frac{w}{R}+\frac{1}{2}\left(\frac{\partial w}{R\partial\theta}\right)^2\right)\\&+D_{11}\left(\frac{\partial\psi_x}{\partial x}\right)+D_{12}\left(\frac{\partial\psi_\theta}{R\partial\theta}\right)+F_{11}\left(\frac{-4}{3h^2}\left(\frac{\partial\psi_x}{\partial x}+\frac{\partial^2 w}{\partial x^2}\right)\right)\\&+F_{12}\left(\frac{-4}{3h^2}\left(\frac{\partial\psi_\theta}{R\partial\theta}+\frac{\partial^2 w}{R^2\partial\theta^2}\right)\right)-M_{xx}^T,\\&M_{\theta\theta}=B_{12}\left(\frac{\partial u}{\partial x}+\frac{1}{2}\left(\frac{\partial w}{\partial x}\right)^2\right)+B_{22}\left(\frac{\partial v}{R\partial\theta}+\frac{w}{R}+\frac{1}{2}\left(\frac{\partial w}{R\partial\theta}\right)^2\right)\\&+D_{12}\left(\frac{\partial\psi_x}{\partial x}\right)+D_{22}\left(\frac{\partial\psi_\theta}{R\partial\theta}\right)+F_{12}\left(\frac{-4}{3h^2}\left(\frac{\partial\psi_x}{\partial x}+\frac{\partial^2 w}{\partial x^2}\right)\right)\\&+F_{22}\left(\frac{-4}{3h^2}\left(\frac{\partial\psi_\theta}{R\partial\theta}+\frac{\partial^2 w}{R^2\partial\theta^2}\right)\right)-M_{\theta\theta}^T,\\&M_{x\theta}=B_{66}\left(\frac{\partial u}{R\partial\theta}+\frac{\partial v}{\partial x}+\frac{\partial w}{\partial x}\frac{\partial w}{R\partial\theta}\right)+D_{66}\left(\frac{\partial\psi_x}{R\partial\theta}+\frac{\partial\psi_\theta}{\partial x}\right)\\&+F_{66}\left(\frac{-4}{3h^2}\left(\frac{\partial\psi_\theta}{\partial x}+\frac{\partial\psi_x}{R\partial\theta}+2\frac{\partial^2 w}{R\partial x\partial\theta}\right)\right),\end{aligned} \tag{39}$$

$$\begin{aligned}&P_{xx}=E_{11}\left(\frac{\partial u}{\partial x}+\frac{1}{2}\left(\frac{\partial w}{\partial x}\right)^2\right)+E_{12}\left(\frac{\partial v}{R\partial\theta}+\frac{w}{R}+\frac{1}{2}\left(\frac{\partial w}{R\partial\theta}\right)^2\right)\\&+F_{11}\left(\frac{\partial\psi_x}{\partial x}\right)+F_{12}\left(\frac{\partial\psi_\theta}{R\partial\theta}\right)+H_{11}\left(\frac{-4}{3h^2}\left(\frac{\partial\psi_x}{\partial x}+\frac{\partial^2 w}{\partial x^2}\right)\right)\\&+H_{12}\left(\frac{-4}{3h^2}\left(\frac{\partial\psi_\theta}{R\partial\theta}+\frac{\partial^2 w}{R^2\partial\theta^2}\right)\right)-P_{xx}^T,\\&P_{\theta\theta}=E_{12}\left(\frac{\partial u}{\partial x}+\frac{1}{2}\left(\frac{\partial w}{\partial x}\right)^2\right)+E_{22}\left(\frac{\partial v}{R\partial\theta}+\frac{w}{R}+\frac{1}{2}\left(\frac{\partial w}{R\partial\theta}\right)^2\right)\\&+F_{12}\left(\frac{\partial\psi_x}{\partial x}\right)+F_{22}\left(\frac{\partial\psi_\theta}{R\partial\theta}\right)+H_{12}\left(\frac{-4}{3h^2}\left(\frac{\partial\psi_x}{\partial x}+\frac{\partial^2 w}{\partial x^2}\right)\right)\\&+H_{22}\left(\frac{-4}{3h^2}\left(\frac{\partial\psi_\theta}{R\partial\theta}+\frac{\partial^2 w}{R^2\partial\theta^2}\right)\right)-P_{\theta\theta}^T,\\&P_{x\theta}=E_{66}\left(\frac{\partial u}{R\partial\theta}+\frac{\partial v}{\partial x}+\frac{\partial w}{\partial x}\frac{\partial w}{R\partial\theta}\right)+F_{66}\left(\frac{\partial\psi_x}{R\partial\theta}+\frac{\partial\psi_\theta}{\partial x}\right)\\&+H_{66}\left(\frac{-4}{3h^2}\left(\frac{\partial\psi_\theta}{\partial x}+\frac{\partial\psi_x}{R\partial\theta}+2\frac{\partial^2 w}{R\partial x\partial\theta}\right)\right),\end{aligned} \tag{40}$$

$$\begin{aligned}&Q_x=A_{44}\left(\frac{\partial w}{\partial x}+\psi_x\right)+D_{44}\left(\frac{-4}{h^2}\left(\psi_x+\frac{\partial w}{\partial x}\right)\right),\\&Q_\theta=A_{55}\left(\frac{\partial w}{R\partial\theta}+\psi_\theta\right)+D_{55}\left(\frac{-4}{h^2}\left(\psi_\theta+\frac{\partial w}{R\partial\theta}\right)\right),\end{aligned} \tag{41}$$

$$\begin{aligned}&K_x=D_{44}\left(\frac{\partial w}{\partial x}+\psi_x\right)+F_{44}\left(\frac{-4}{h^2}\left(\psi_x+\frac{\partial w}{\partial x}\right)\right),\\&K_\theta=D_{55}\left(\frac{\partial w}{R\partial\theta}+\psi_\theta\right)+F_{55}\left(\frac{-4}{h^2}\left(\psi_\theta+\frac{\partial w}{R\partial\theta}\right)\right),\end{aligned} \tag{42}$$

where

$$A_{ij} = \int_{-h/2}^{h/2} C_{ij} dz, \qquad (i, j = 1,2,6) \tag{43a}$$

$$B_{ij} = \int_{-h/2}^{h/2} C_{ij} z dz, \tag{43b}$$

$$D_{ij} = \int_{-h/2}^{h/2} C_{ij} z^2 dz, \tag{43c}$$

$$E_{ij} = \int_{-h/2}^{h/2} C_{ij} z^3 dz, \tag{43d}$$

$$F_{ij} = \int_{-h/2}^{h/2} C_{ij} z^4 dz, \tag{43e}$$

$$H_{ij} = \int_{-h/2}^{h/2} C_{ij} z^6 dz, \tag{43f}$$

Furthermore, $\left(N_{xx}^T, N_{\theta\theta}^T\right)$ is thermal force which is

$$\begin{Bmatrix} N_{xx}^T \\ N_{\theta\theta}^T \end{Bmatrix} = \int_{-h/2}^{h/2} \begin{Bmatrix} C_{11}(T)\alpha_{xx} + C_{12}(T)\alpha_{\theta\theta} \\ C_{21}(T)\alpha_{xx} + C_{22}(T)\alpha_{\theta\theta} \end{Bmatrix} \Delta T \, dz, \tag{44}$$

Substituting Eqs. (38) to (42) into Eqs. (30) to (34), the governing equations are derived in Appendix A.

4. Solution method

4.1 DQ

DQ method approximate the partial derivative of a function, with respect to a spatial variable at a given discrete point, as a weighted linear sum of the function values at all discrete points chosen in the solution domain of the spatial variable. However, the n^{th}-order partial derivative of $F(x, \theta)$ with respect to x, the m^{th}-order with respect to θ and the $(n + m)^{\text{th}}$-order with respect to both x and θ may be expressed discretely at the point (x_i, θ_i) as (Kolahchi *et al*. 2016a, 2016b)

$$\frac{d^n F(x_i, \theta_j)}{dx^n} = \sum_{k=1}^{N_x} A_{ik}^{(n)} F(x_k, \theta_j) \qquad n = 1,..., N_x - 1, \tag{45}$$

$$\frac{d^m F(x_k, \theta_j)}{d\theta^m} = \sum_{l=1}^{N_\theta} B_{jl}^{(m)} F(x_k, \theta_j) \qquad m = 1,..., N_\theta - 1, \tag{46}$$

$$\frac{d^{n+m} F(x_k, \theta_j)}{dx^n d\theta^m} = \sum_{k=1}^{N_x} \sum_{l=1}^{N_\theta} A_{ik}^{(n)} B_{jl}^{(m)} F(x_k, \theta_j), \tag{47}$$

where N_x and N_θ are the positions of the grid points which are calculated using Chebyshev polynomials (Kolahchi *et al*. 2016a, 2016b); $A_{ik}^{(n)}$ and $B_{jl}^{(m)}$ are the weighting coefficients which can be obtained using the following formula

$$A^{(1)}{}_{ij} = \frac{P(x_i)}{(x_i - x_j)P(x_j)}, \tag{48}$$

where

$$P(x_i) = \prod_{j=1, j\neq i}^{N_x} (x_i - x_j); \qquad for\ j = 1,2,3,...N_x \tag{49}$$

and when $i=j$

$$A_{ii}^{(1)} = -\sum_{j=1, j\neq 1}^{N_x} A_{ij}^{(1)}, \qquad for\ i = 1,2,..., N_x \tag{50}$$

In a similar manner, the weighting coefficients for θ-direction can be obtained. The weighting coefficients for the second, third and fourth derivatives can be determined via matrix multiplication.

4.2 IQ

IQ is also based on the analysis of a high-order polynomial approximation and of a linear vector space. As a general case it is assumed that the integral off(x) over a part of the whole domain can be approximated by a linear combination of all the functional values in the whole domain in the form (Shu *et al*. 1995)

$$\int_{x_i}^{x_j} f(x)dx = \sum_{k=1}^{N_x} C_k^{ij} f(x_k), \qquad with\ C_k^{ij} = w_{jk}^I - w_{ik}^I, \tag{51}$$

where x_i and x_j are numbers that can be altered; W^I=A^{-1} which we have

$$a_{ij} = \frac{x_i - c}{x_j - c} A_{ij}^{(1)} \quad when\ i \neq j \tag{52}$$

$$a_{ii} = A_{ii}^{(1)} + \frac{1}{x_i - c} \quad when\ i \neq j \tag{53}$$

where $A_{ij}^{(1)}$ is the weighting coefficient of the first-order derivative in DQ; c is a constant which taken as 0.01. However, using DQ-IQ methods, the motion equations can be written in a compact matrix form as follows

$$[K_L + K_{NL}][d(t)] + [C][\dot{d}(t)] + [M][\ddot{d}(t)] = [Q(t)], \tag{54}$$

where $[d]=[u\ v\ w\ \psi_x\ \psi_y]^T$; $[K_L]$ and $[K_{NL}]$ are respectively, linear and nonlinear stiffness matrixes; $[C]$ is damp matrix and $[M]$ is the mass matrix.

4.3 Newmark time integration scheme

Here, the average acceleration method of Newmark-β (Simsek and Kocatu¨rk 2009) in conjunction with an iteration method is used. Based on this method, the above time domain equations (Eq. (54)) can be reduced to the following set of nonlinear algebraic equations

$$K^*(d_{i+1}) = Q_{i+1}, \tag{55}$$

where subscript i+1 shows the time t=t_{i+1}; $K^*(d_{i+1})$ is the effective stiffness matrix and Q_{i+1} is the effective load vector, which can be written as

$$K^*(d_{i+1}) = K_L + K_{NL}(d_{i+1}) + \alpha_0 M + \alpha_1 C, \tag{56}$$

$$\begin{aligned} Q_{i+1}^* &= Q_{i+1} + M\left(\alpha_0 d_i + \alpha_2 \dot{d}_i + \alpha_3 \ddot{d}_i\right) \\ &+ C\left(\alpha_1 d_i + \alpha_4 \dot{d}_i + \alpha_5 \ddot{d}_i\right), \end{aligned} \tag{57}$$

Table 1 Temperature-dependent material properties of (10, 10) SWCNT (L=9.26 nm, R=0.68 nm, h=0.067 nm, $\upsilon_{12}^{CNT}=0.175$)

Temperature (K)	E_{11}^{CNT} (TPa)	E_{22}^{CNT} (TPa)	G_{12}^{CNT} (TPa)	α_{12}^{CNT} ($10^{-6}/K$)	α_{22}^{CNT} ($10^{-6}/K$)
300	5.6466	7.0800	1.9445	3.4584	5.1682
500	5.5308	6.9348	1.9643	4.5361	5.0189
700	5.4744	6.8641	1.9644	4.6677	4.8943

where

$$\alpha_0=\frac{1}{\chi\Delta t^2},\quad \alpha_1=\frac{\gamma}{\chi\Delta t},\quad \alpha_2=\frac{1}{\chi\Delta t},$$
$$\alpha_3=\frac{1}{2\chi}-1,\quad \alpha_4=\frac{\gamma}{\chi}-1,\alpha_5=\frac{\Delta t}{2}\left(\frac{\gamma}{\chi}-2\right), \tag{58}$$
$$\alpha_6=\Delta t\left(1-\gamma\right),\qquad \alpha_7=\Delta t\gamma,$$

where γ=0.5 and χ=0.25 (Simsek and Kocatu¨rk 2009). Based on iteration method, Eq. (55) at any fixed time can be solved and then the new acceleration and velocity vectors, respectively can be obtained as follows

$$\ddot{d}_{i+1}=\alpha_0(d_{i+1}-d_i)-\alpha_2\dot{d}_i-\alpha_3\ddot{d}_i, \tag{59}$$

$$\dot{d}_{i+1}=\dot{d}_i+\alpha_6\ddot{d}_i+\alpha_7\ddot{d}_{i+1}, \tag{60}$$

Noted that the above procedures should be repeated for each time step.

5. Numerical results and discussion

In the numerical results, dynamic response of FG-CNT reinforced pipes conveying viscous fluid under moving load is investigated. The dynamic deflection of structure is calculated using DQ-IQ methods as well as Newmark method. A pipe with length to radius ratio L/R=5 and thickness to radius ratio h/R=0.02 is considered which is made from Poly methyl methacrylate (PMMA) with constant Poisson's ratios of ν_m=0.34, temperature-dependent thermal coefficient of α_m=(1+0.005ΔT)×$10^{-6}/K$, and temperature-dependent Young moduli of E_m=(3.52−0.0034T)GPa in which $T=T_0+\Delta T$ and T_0=300 K (room temperature). In addition, (10, 10) SWCNTs are selected as reinforcements with the material properties listed in Table 1 (Raminnea *et al*. 2016). The CNT reinforced pipes are considered with two kinds of boundary conditions: two edges simply supported (SS) or clamped (CC) (Raminnea *et al*. 2016).

5.1 DQM convergence

The convergence and accuracy of the proposed method in obtaining the maximum dynamic displacement of pipe are shown in Fig. 2. It can be seen that with increasing the grid point numbers, the magnitude of dynamic displacement increases until in N=17, the results become converge. However, in this work, the number of grid points is taken 17.

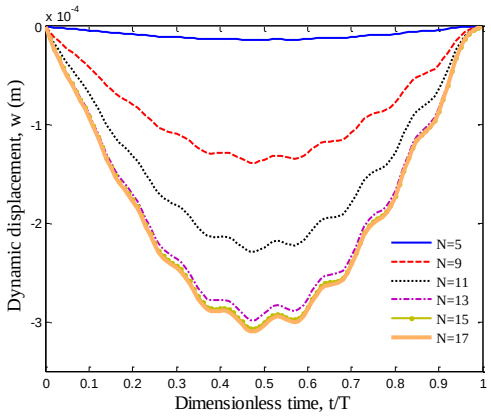

Fig. 2 Convergence and accuracy of proposed methods

Table 2 Comparison of the dynamic displacement of present work and Bayat *et al*. (2016)

T	V_{CNT}=0.12			V_{CNT}=0.17			V_{CNT}=0.28		
	UD	FGA	FGX	UD	FGA	FGX	UD	FGA	FGX
300, Bayat *et al.* (2016)	0.1398	0.1423	0.1366	0.1072	0.1083	0.1048	0.0976	0.0966	0.0938
400, Bayat *et al.* (2016)	0.1758	0.1827	0.1716	0.1269	0.1301	0.1240	0.1148	0.1161	0.01107
500, Bayat *et al.* (2016)	0.7742	0.2916	0.7377	0.2020	0.2279	0.1997	0.1691	0.1926	0.1694
300, present	0.1394	0.1421	0.1361	0.1075	0.1087	0.1043	0.0971	0.0963	0.0941
400, present	0.1756	0.1829	0.1712	0.1264	0.1306	0.1246	0.1142	0.1159	0.1102
500, present	0.7740	0.2911	0.7374	0.2023	0.2273	0.1994	0.1695	0.1922	0.1698

5.2 Validation

To the best author's knowledge, there is not any similar publication for dynamic response of FG-CNT reinforced pipes conveying fluid under moving load. However, neglecting fluid and moving load, presented results are compared with the work of Bayat *et al*. (2016). Considering the contact force the same as Bayat *et al*. (2016) with the velocity of 3 m/s, the results are shown in Table 2 for different CNT volume percent and distribution types. As can be seen, the obtained results are the close to those expressed in Bayat *et al*. (2016), indicating validation of our work.

5.3 Dynamic response of structure

CNT volume percent and distribution type are shown in Figs. 3 and 4 on the dynamic response of the pipe. From Fig. 3, it can be found that increasing the CNTs volume fraction decreases the magnitude of the maximum dynamic deflection due to increase in stiffness of structure. In Fig. 4, four types of CNT distribution are considered. As can be seen, the magnitude of dynamic displacement of FGV- and

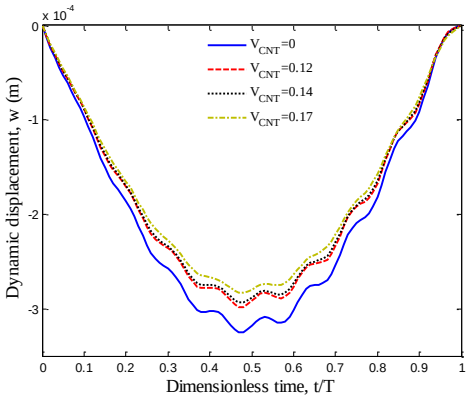

Fig. 3 Effects of CNT volume percent on the maximum dynamic deflection of structure

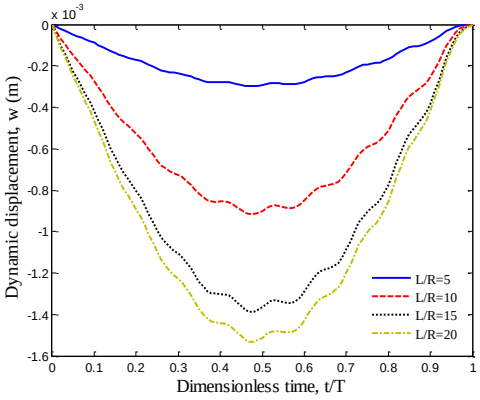

Fig. 5 Effects of length to radius ratio on the maximum dynamic deflection of structure

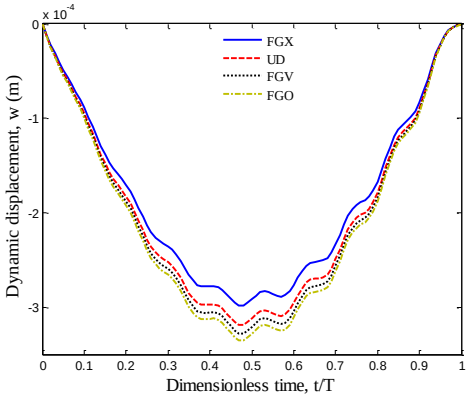

Fig. 4 Effects of CNT distribution types on the maximum dynamic deflection of structure

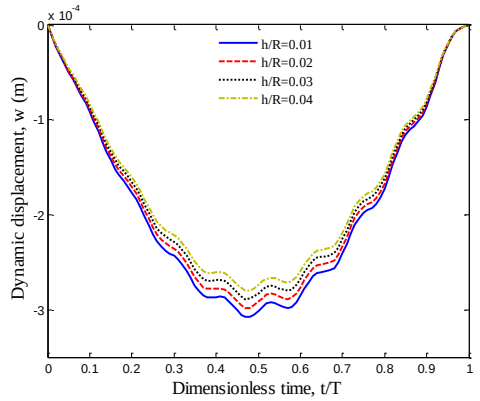

Fig. 6 Effects of thickness to radius ratio on the maximum dynamic deflection of structure

FGO-CNTRC pipes are higher than those of UD-CNT reinforced pipe while the FGX-CNT reinforced pipe has lower dynamic displacement with respect to three other cases. For example, the FGX-CNT reinforced pipe reduces the maximum deflection of the structure 7 percent with respect to UD ones. However, it can be concluded that CNTs distribution close to top and bottom are more efficient than those distributed nearby the mid-plane for increasing the stiffness of pipes.

In order to show the effect of geometrical parameters of pipe on the dynamic response of structure, Figs. 5 and 6 are plotted. Fig. 5 illustrates the maximum dynamic deflection of pipe for different length to radius ratios. It is apparent that this geometrical parameter can significantly change the dynamic deflection of the FG-CNT-reinforced pipe. It can be found that with increasing the length to radius ratio, the magnitude of dynamic deflection increases. For example, changing the length to radius ratio from 10 to 20 increases 64.85% the maximum dynamic deflection of the pipe. It is due to the fact that with increasing the length to radius ratio, the structure becomes softer. Furthermore, by increasing length to radius ratio, the difference between the maximum deflections for the pipe decreases. The effect of thickness to radius ratio on the dynamic deflection of pipe is demonstrated in Fig. 6. It is obvious that the dynamic deflection of pipe is decreased with increasing thickness to radius ratio due to increase in the stiffness of system.

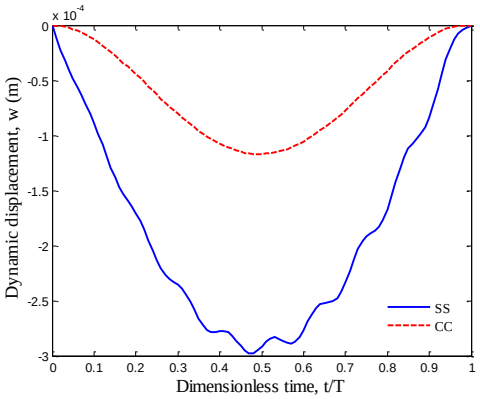

Fig. 7 Effects of boundary conditions on the maximum dynamic deflection of structure

Fig. 7 indicates the maximum dynamic deflection of structure for two boundary conditions of SS and CC. As can be seen, the shape of dynamic response obtained by CC pipe under moving load is smoother that those predicted by SS one. It is also concluded that the dynamic deflection of CC pipe is lower than SS pipe. It is because the CC boundary conditions make the structure stiffer and more rigid.

The effect of velocity and acceleration of moving load on the maximum dynamic deflection of pipe is presented in Fig. 8. As it is obvious, the time or location of maximum displacement accelerated and decelerated motion of moving

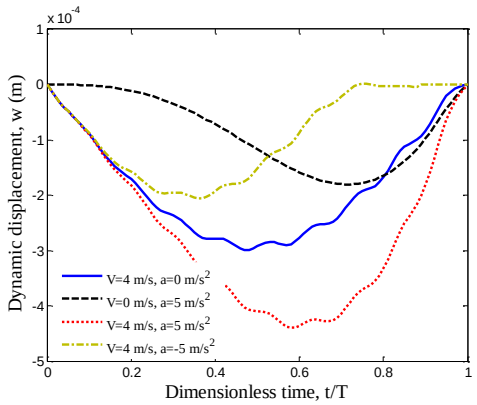

Fig. 8 Effects of velocity and acceleration of moving load on the maximum dynamic deflection of structure

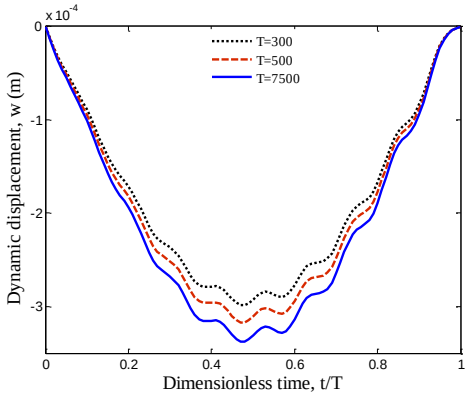

Fig. 9 Effects of temperature changes on the maximum dynamic deflection of structure

load are different. When the moving load is decelerated, the maximum displacement is occurred in the midpoint of pipe approximately. In the accelerated motion of the moving load, two cases are considered. In both cases, the maximum displacement is occurred at the right side of the midpoint. In addition, in the case of zero velocity, the shape of dynamic response is smoother that the cases non zero moving load velocity. Furthermore, considering negative acceleration leads to decrease in the maximum displacement of the structure with respect to the case of positive and zero accelerations. It is also concluded when the acceleration of moving load is negative, the dynamic deflection reach to zero after an especial time.

Fig. 9 indicates the effect of temperature changes on the maximum dynamic displacement of pipe as a function of moving load velocity. As can be seen, with increasing the temperature change, the values of the maximum dynamic displacement are increased. It is due to the fact that with increasing the temperature changes, the structure becomes softer.

The maximum dynamic displacement of pipe versus moving load velocity is plotted in Fig. 10 for different fluid velocities. As can be seen, the maximum dynamic displacement of the pipe shows a predominant peaks, which correspond to the critical moving load velocity. In addition, with increasing the fluid velocity, the critical velocity of moving load decreases. For example, for the pipe without

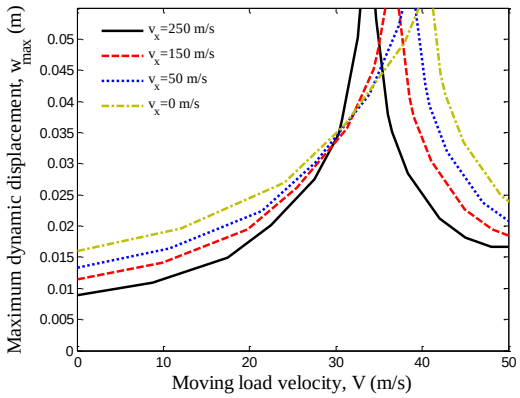

Fig. 10 Effects of fluid velocity on the critical moving load velocity

fluid, the critical moving load velocity is about 40 m/s while for the pipe for fluid velocity of 250 m/s, the critical moving load velocity is about 34 m/s.

6. Conclusions

Dynamics response of nanocomposite pipes conveying fluid under the moving load was presented in this paper. Considering pipe reinforced by FG-CNT, temperature-dependent material properties of pipe, viscous fluid flow in the pipe, accelerated moving load, Reddy shear deformation theory for modeling and utilizing DQ, IQ and Newmark methods for solution were the main contributions of this work. The effects of CNT volume percent and distribution type, boundary conditions, geometrical parameters, velocity and acceleration of moving load were shown on the dynamic response of structure. Some main conclusions especially for the novelties of this work are:

1. Increasing the CNTs volume fraction decreases the magnitude of the maximum dynamic deflection.
2. The magnitude of dynamic displacement of FGV- and FGO-CNTRC pipes are higher than those of UD-CNT reinforced pipe while the FGX-CNT reinforced pipe has lower dynamic displacement with respect to three other cases.
3. The FGX-CNT reinforced pipe reduces the maximum deflection of the structure 7 percent with respect to UD ones.
4. It was apparent that the length to radius ratio changes the dynamic deflection of the FG-CNT-reinforced pipe so that with increasing the length to radius ratio, the magnitude of dynamic deflection increases. For example, changing the length to radius ratio from 10 to 20 increases 64.85% the maximum dynamic deflection of the pipe.
5. Dynamic response obtained by CC pipe under moving load is smoother that those predicted by SS one.
6. When the moving load was decelerated, the maximum displacement was occurred in the midpoint of pipe approximately. In the accelerated motion of the moving load, the maximum displacement is occurred at the right side of the midpoint.

7. Considering negative acceleration leads to decrease in the maximum displacement of the structure with respect to the case of positive and zero accelerations.

8. It was also concluded when the acceleration of moving load is negative, the dynamic deflection reach to zero after an especial time.

9. With increasing the temperature change, the values of the maximum dynamic displacement were increased

Finally, it is hoped that the presented results would be helpful for study and design of piped subjected to moving load.

References

Attar, M., Karrech, A. and egenauer-LieK, R. (2015), "Dynamic response of cracked Timoshenko beams on elastic foundations under moving harmonic loads", *J. Vib. Control*, **20**: 1077546315580470.

Bayat, M.R., Rahmani, O. and Mosavi Mashhadi, M. (2016), "Nonlinear Low-Velocity Impact Analysis of Functionally Graded Nanotube-Reinforced Composite Cylindrical Shells in Thermal Environments", *Polymer Compos.*, In press.

Bespalova, E.I., (2007), "Reaction of an anisotropic cylindrical shell to a moving load", *Int. J. Appl. Mech.*, **43**: 425–31.

Castro Jorge, P., Simões, F.M.F. and Pinto da Costa, A. (2015), "Dynamics of beams on non-uniform nonlinear foundations subjected to moving loads", *Comput. Struct.*, **148**: 24-34.

Gbadeyan, J.A. and Dada, M.S. (2011), "A comparison of dynamic responses of three versions of moving load problem involving elastic rectangular plates", *J. Vib. Control*, **17**: 903-915

Chen, J.S. and Tsai, S.M. (2016), "Sandwich structures with periodic assemblies on elastic foundation under moving loads", *J. Vib. Control*, **22**: 2519-2529.

Chonan, S. (1981), "Moving load on a two-layered cylindrical shell with imperfect bonding", *The J. Acoust. Soc. Americ.*, **69**: 1015–20.

Ding, L., Zhu, H.P. and Wu, L. (2016), "Effects of axial load and structural damping on wave propagation in periodic Timoshenko beams on elastic foundations under moving loads", *Phys. Lett. A*, **380**: 2335-2341.

Eftekhari, S.A. and Jafari, A.A. (2012), "Vibration of an initially stressed rectangular plate due to an accelerated traveling mass", *Scient. Iran. A*, **19**: 1195–1213.

Eftekhari, S.A. (2016), "Differential quadrature procedure for in-plane vibration analysis of variable thickness circular arches traversed by a moving point load", *Appl. Math. Model*, **40**: 4640-4663.

Ghafoori, E. and Asghari, M. (2010), "Dynamic analysis of laminated composite plates traversed by a moving mass based on a first-order theory", *Compos. Struct.*, **92**: 1865–76.

He, W.Y. and Zhu, S. (2016), "Moving load-induced response of damaged beam and its application in damage localization", *J. Vib. Control*, **22**: 3601-3617.

Huang, C.C. (1976), "Moving loads on elastic cylindrical shells", *J. Sound Vib.*, **49**: 215–20

Huang, C.S., Tseng, Y.P. and Hung, C.L. (2000), "An accurate solution for the responses of circular curved beams subjected to a moving load", *Int. J. Numeric. Meth. Eng.*, **48**: 1723–1740.

Kaur, T., Singh, A.K., Chattopadhyay, A. and Sharma, S.K. (2016), "Dynamic response of normal moving load on an irregular fiber-reinforced half-space", *J. Vib. Control*, **22**: 77-88.

Kolahchi, R., Safari, M. and Esmailpour, M. (2016a), "Dynamic stability analysis of temperature-dependent functionally graded CNT-reinforced visco-plates resting on orthotropic elastomeric medium", *Compos. Struct.*, **150**: 255-265.

Kolahchi, R., Hosseini, H. and Esmailpour, M. (2016b), "Differential cubature and quadrature-Bolotin methods for dynamic stability of embedded piezoelectric nanoplates based on visco-nonlocal-piezoelasticity theories", *Compos. Struct*, **157**: 174–186.

Law, S.S., Bu, J.Q., Zhu, X.Q. and Chan, S.L. (2007), "Moving load identification on a simply supported orthotropic plate", *Int. J. Mech. Sci.*, **49**: 1262–1275.

Liew, K.M., Lei, Z.X., Yu, J.L. and Zhang, L.W. (2014), "Postbuckling of carbon nanotube-reinforced functionally graded cylindrical panels under axial compression using a meshless approach", *Comput. Meth. Appl. Mech. Eng.*, **268**: 1-17.

Malekzadeh, P. and Heydarpour, Y. (2012), "Response of functionally graded cylindrical shells under moving thermo-mechanical loads", *Thin-Wall. Struct*, **58**: 51–66.

Malekzadeh, P. and Monajjemzadeh, S.M. (2013), "Dynamic response of functionally graded plates in thermal environment under moving load", *Compos.: Part B*, **45**: 1521–33.

Malekzadeh, P. and Daraie, M. (2014), "Dynamic analysis of functionally graded truncated conical shells subjected to asymmetric moving loads", *Thin-Wall. Struct.*, **84**: 1–13.

Panneton, R., Berry, A. and Laville, F. (1995), "Vibration and sound radiation of a cylindricalshell under a circumferentially moving load",. *The J. Acoust. Soc. Americ.*, **98**: 2165–73.

Raminnea, M., Biglari, H. and Vakili Tahami, F. (2016), "Nonlinear higher order Reddy theory for temperaturedependent vibration and instability of embedded functionally graded pipes conveying fluid-nanoparticle mixture", *Struct. Eng. Mech.*, **59**: 153-186.

Reddy, J.N. (1984), "A Simple Higher Order Theory for Laminated Composite Plates", *J. Appl. Mech.*, **51**: 745–752.

Ruzzene, M. and Baz, A, (2006), "Dynamic stability of periodic shells with moving loads", *J. Sound Vib.*, **296**: 830–44.

Sadeghi, M.H. and Karimi-Dona, M.H. (2011), "Dynamic behavior of afluid conveying pipe subjected to a moving sprung masse An FEM-state space approach", *Int. J. Press. Vess. Pip.*, **88**: 123e131.

Sheng, C.X. (1985), "Forced vibrations of elastic shallow shell due to the moving mass", *Appl. Math. Mech.*, **6**: 231–8.

Sheng, G.G. and Wang, X. (2009), "Studies on dynamic behavior of functionally graded cylindrical shells with PZT layers under moving loads", *J. Sound Vib.*, **323**: 772–789.

Sheng, G.G. and Wang, X. (2010), "Response and control of functionally graded laminated piezoelectric shells under thermal shock and moving loadings", *Compos. Struct.*, **93**: 132–41.

Shu, C., Chew, Y.T. and Richards, E. (1995), "Generalized differential and integral quadrature and their application to solve boundary layer equations" *Int. J. Numeric. Meth. Fluids*, **21**: 723-733.

Simsek, M. and Kocatu¨rk, T., (2009), "Nonlinear dynamic analysis of an eccentrically prestressed damped beam under a concentrated moving harmonic load", *J. Sound Vib.*, **320**: 235–253.

Sing, V.P., Dwivedi, J.P. and Upahyay, P.C. (1999), "Non-axisymmetric dynamic response of buried orthotropic cylindrical shells under moving load", *Struct. Eng. Mech.*, **8**: 39–51.

Sofiyev, A.H. (2010), "Dynamic response of an FGM cylindrical shell under moving loads", *Compos. Struct*, **93**: 58–66.

Song, Q., Shi, J., Liu, Z. and Wan, Y. (2016), "Dynamic analysis of rectangular thin plates of arbitrary boundary conditions under moving loads", *Int. J. Mech. Sci.*, **117**: 16-29.

Sudheesh Kumar, C.P., Sujath, C. and Shankar, K. (2015), "Vibration of simply supported beams under a single moving

load: A detailed study of cancellation phenomenon", *Int. J. Mech. Sci.*, **99**: 40-47.

Wang, D., Zhang, W. and Zhu, J. (2016), "A moving bounds strategy for the parameterization of geometric design variables in the simultaneous shape optimization of curved shell structures and openings", *Finite Elem. Anal. Des.*, **120**: 80-9.

Wang, Y. and Wu, D. (2016), "Thermal effect on the dynamic response of axially functionally graded beam subjected to a moving harmonic load", *Acta Astronaut.*, **127**: 17-181.

Wu, J.S., Lee, M.L. and Lai, T.S. (1987), "The dynamic analysis of a flat plate under a moving load by the finite element method", *Int. J. Numeric. Meth. Eng.*, **24**: 743–762.

Wu, J.S. and Chen, C.C. (1989), "The dynamic analysis of a suspended cable due to a moving load", *Int. J. Numeric. Meth. Eng.*, **28**: 2361–2381.

Yang, J., Chen, Y., Xiang, Y. and Jia, X.L. (2008), "Free and forced vibration of a cracked FGM beam under an axial force and a moving load, *J. Sound Vib.*, **312**: 166–181.

Yu, D., Wen, J., Shen, H. and Wen, X. (2012), "Propagation of steady-state vibration in periodic pipes conveying fluid on elastic foundations with external moving loads", *Phys. Lett. A*, **376**: 3417–3422.

Zhu, X.Q. and Law, S.S. (2003), "Dynamic behavior of orthotropic rectangular plates under moving loads", *J. Eng. Mech.*, **129**: 79–87.

CC

Appendix A

$$
\begin{aligned}
&\delta u: A_{11}\left(\frac{\partial^2 u}{\partial x^2}+\frac{\partial w}{\partial x}\frac{\partial^2 w}{\partial x^2}\right)+A_{12}\left(\frac{\partial^2 v}{R\partial\theta\partial x}+\frac{\partial w}{R\partial x}+\frac{\partial w}{R\partial\theta}\frac{\partial^2 w}{R\partial\theta\partial x}\right)\\
&+B_{11}\left(\frac{\partial^2\psi_x}{\partial x^2}\right)+B_{12}\left(\frac{\partial^2\psi_\theta}{R\partial\theta\partial x}\right)+E_{11}\left(\frac{-4}{3h^2}\left(\frac{\partial^2\psi_x}{\partial x^2}+\frac{\partial^3 w}{\partial x^3}\right)\right)\\
&+E_{12}\left(\frac{-4}{3h^2}\left(\frac{\partial^2\psi_\theta}{R\partial\theta\partial x}+\frac{\partial^3 w}{R^2\partial x\,\partial\theta^2}\right)\right)+B_{66}\left(\frac{\partial^2\psi_x}{R^2\partial\theta^2}+\frac{\partial^2\psi_\theta}{R\partial\theta\partial x}\right)\\
&+A_{66}\left(\frac{\partial^2 u}{R^2\partial\theta^2}+\frac{\partial^2 v}{R\partial\theta^2}+\frac{\partial^2 w}{R\partial\theta\partial x}\frac{\partial w}{R\partial\theta}+\frac{\partial w}{\partial x}\frac{\partial^2 w}{R^2\partial\theta^2}\right)\\
&+E_{66}\left(\frac{-4}{3h^2}\left(\frac{\partial^2\psi_\theta}{R\partial\theta\partial x}+\frac{\partial^2\psi_x}{R^2\partial\theta^2}+2\frac{\partial^3 w}{R^2\partial x\,\partial\theta^2}\right)\right)\\
&=I_0\frac{\partial^2 u}{\partial t^2}+J_1\frac{\partial^2\psi_x}{\partial t^2}-\frac{4I_3}{h^2}\frac{\partial^3 w}{\partial t^2\partial x},
\end{aligned}
\tag{A1}
$$

$$
\begin{aligned}
&\delta v: A_{12}\left(\frac{\partial^2 u}{R\partial\theta\partial x}+\frac{\partial w}{\partial x}\frac{\partial^2 w}{R\partial\theta\partial x}\right)+A_{22}\left(\frac{\partial^2 v}{R^2\partial\theta^2}+\frac{\partial w}{R\partial\theta}+\frac{\partial w}{R\partial\theta}\frac{\partial^2 w}{R^2\partial\theta^2}\right)\\
&+B_{12}\left(\frac{\partial^2\psi_x}{R\partial\theta\partial x}\right)+B_{22}\left(\frac{\partial^2\psi_\theta}{R^2\partial\theta^2}\right)+E_{12}\left(\frac{-4}{3h^2}\left(\frac{\partial^2\psi_x}{R\partial\theta\partial x}+\frac{\partial^3 w}{R\partial\theta\partial x^2}\right)\right)\\
&+E_{22}\left(\frac{-4}{3h^2}\left(\frac{\partial^2\psi_\theta}{R^2\partial\theta^2}+\frac{\partial^3 w}{R^3\partial\theta^3}\right)\right)+B_{66}\left(\frac{\partial^2\psi_x}{R\partial\theta\partial x}+\frac{\partial^2\psi_\theta}{\partial x^2}\right)\\
&+A_{66}\left(\frac{\partial^2 u}{R\partial\theta\partial x}+\frac{\partial^2 v}{\partial x^2}+\frac{\partial^2 w}{\partial x^2}\frac{\partial w}{R\partial\theta}+\frac{\partial w}{\partial x}\frac{\partial^2 w}{R\partial\theta\partial x}\right)\\
&+E_{66}\left(\frac{-4}{3h^2}\left(\frac{\partial^2\psi_\theta}{\partial x^2}+\frac{\partial^2\psi_x}{R\partial\theta\partial x}+2\frac{\partial^3 w}{R\partial x^2\partial\theta}\right)\right)\\
&=I_0\frac{\partial^2 v}{\partial t^2}+J_1\frac{\partial^2\psi_\theta}{\partial t^2}-\frac{4I_3}{h^2}\frac{\partial^3 w}{R\partial t^2\partial\theta},
\end{aligned}
\tag{A2}
$$

$$
\begin{aligned}
&\delta w: A_{44}\left(\frac{\partial^2 w}{\partial x^2}+\frac{\partial\psi_x}{\partial x}\right)+D_{44}\left(\frac{-4}{h^2}\left(\frac{\partial\psi_x}{\partial x}+\frac{\partial^2 w}{\partial x^2}\right)\right)\\
&+A_{55}\left(\frac{\partial^2 w}{R^2\partial\theta^2}+\frac{\partial\psi_\theta}{R\partial\theta}\right)+D_{55}\left(\frac{-4}{h^2}\left(\frac{\partial\psi_\theta}{R\partial\theta}+\frac{\partial^2 w}{R^2\partial\theta^2}\right)\right)\\
&+\frac{\partial}{\partial x}\left(N_{xx}\frac{\partial w}{\partial x}\right)+\frac{\partial}{R\partial\theta}\left(N_{\theta\theta}\frac{\partial w}{R\partial\theta}\right)\\
&-\frac{4}{h^2}\left(\left(D_{44}\left(\frac{\partial^2 w}{\partial x^2}+\frac{\partial\psi_x}{\partial x}\right)+F_{44}\left(\frac{-4}{h^2}\left(\frac{\partial^2 w}{\partial x^2}+\frac{\partial\psi_x}{\partial x}\right)\right)\right)\right.\\
&\left.+\left(D_{55}\left(\frac{\partial^2 w}{R^2\partial\theta^2}+\frac{\partial\psi_\theta}{R\partial\theta}\right)+F_{55}\left(\frac{-4}{h^2}\left(\frac{\partial^2 w}{R^2\partial\theta^2}+\frac{\partial\psi_\theta}{R\partial\theta}\right)\right)\right)\right)\\
&+\frac{4}{3h^2}\left[E_{11}\left(\frac{\partial^3 u}{\partial x^3}+\left(\frac{\partial^2 w}{\partial x^2}\right)^2+\frac{\partial w}{\partial x}\frac{\partial^3 w}{\partial x^3}\right)\right.\\
&+E_{12}\left(\frac{\partial^3 v}{R\partial\theta\partial x^2}+\frac{\partial^2 w}{R\partial x^2}+\left(\frac{\partial w}{R\partial\theta}\right)^2+\frac{\partial w}{R\partial\theta}\frac{\partial^3 w}{R\partial x^2\partial\theta}\right)\\
&+F_{11}\left(\frac{\partial^3\psi_x}{\partial x^3}\right)+F_{12}\left(\frac{\partial^3\psi_\theta}{R\partial\theta\partial x^2}\right)+H_{11}\left(\frac{-4}{3h^2}\left(\frac{\partial^3\psi_x}{\partial x^3}+\frac{\partial^4 w}{\partial x^4}\right)\right)\\
&+H_{12}\left(\frac{-4}{3h^2}\left(\frac{\partial^3\psi_\theta}{R\partial\theta\partial x^2}+\frac{\partial^4 w}{R^2\partial\theta^2\partial x^2}\right)\right)+2E_{66}\left(\frac{\partial^3 u}{R^2\partial x\,\partial\theta^2}+\frac{\partial^3 v}{R\partial\theta\partial x^2}\right.\\
&\left.+\frac{\partial^3 w}{R\partial\theta\partial x^2}\frac{\partial w}{R\partial\theta}+\frac{\partial^2 w}{\partial x^2}\frac{\partial^2 w}{R^2\partial\theta^2}+\frac{\partial^3 w}{R^2\partial\theta^2\partial x}\frac{\partial w}{\partial x}\right)\\
&+2F_{66}\left(\frac{\partial^3\psi_x}{R^2\partial x\,\partial\theta^2}+\frac{\partial^3\psi_\theta}{R\partial x^2\partial\theta}\right)+F_{12}\left(\frac{\partial^3\psi_x}{R^2\partial\theta^2\partial x}\right)+F_{22}\left(\frac{\partial^3\psi_\theta}{R^3\partial\theta^3}\right)\\
&+2H_{66}\left(\frac{-4}{3h^2}\left(\frac{\partial^3\psi_\theta}{R\partial x^2\partial\theta}+\frac{\partial^3\psi_x}{R^2\partial x\,\partial\theta^2}+2\frac{\partial^3 w}{R^2\partial x^2\partial\theta^2}\right)\right)\\
&+E_{12}\left(\frac{\partial^3 u}{R^2\partial\theta^2\partial x}+\left(\frac{\partial^2 w}{R\partial x\,\partial\theta}\right)^2+\frac{\partial w}{\partial x}\frac{\partial^3 w}{R^2\partial x\,\partial\theta^2}\right)\\
&+E_{22}\left(\frac{\partial^3 v}{R^3\partial\theta^3}+\frac{\partial^2 w}{R^3\partial\theta^2}+\left(\frac{\partial w}{R\partial\theta}\right)^2+\frac{\partial w}{R\partial\theta}\frac{\partial^3 w}{R^3\partial\theta^3}\right)\\
&+H_{12}\left(\frac{-4}{3h^2}\left(\frac{\partial^3\psi_x}{R^2\partial\theta^2\partial x}+\frac{\partial^4 w}{R^2\partial\theta^2\partial x^2}\right)\right)+H_{22}\left(\frac{-4}{3h^2}\left(\frac{\partial^3\psi_\theta}{R^3\partial\theta^3}+\frac{\partial^4 w}{R^4\partial\theta^4}\right)\right)\\
&-\frac{A_{12}}{R}\left(\frac{\partial u}{\partial x}+\frac{1}{2}\left(\frac{\partial w}{\partial x}\right)^2\right)-\frac{A_{22}}{R}\left(\frac{\partial v}{R\partial\theta}+\frac{w}{R}+\frac{1}{2}\left(\frac{\partial w}{R\partial\theta}\right)^2\right)-\frac{B_{12}}{R}\left(\frac{\partial\psi_x}{\partial x}\right)\\
&\left.-B_{22}\left(\frac{\partial\psi_\theta}{R^2\partial\theta}\right)-E_{12}\left(\frac{-4}{3h^2R}\left(\frac{\partial\psi_x}{\partial x}+\frac{\partial^2 w}{\partial x^2}\right)\right)-E_{22}\left(\frac{-4}{3h^2R}\left(\frac{\partial\psi_\theta}{R\partial\theta}+\frac{\partial^2 w}{R^2\partial\theta^2}\right)\right)\right]\\
&+\left[-\rho_f h_f\left(\frac{\partial^2 w}{\partial t^2}+2v_x\frac{\partial^2 w}{\partial x\,\partial t}+v_x^2\frac{\partial^2 w}{\partial x^2}\right)+\frac{h_f}{R^2}\frac{\partial}{\partial\theta}\left(\mu\left(\frac{\partial^2 w}{\partial\theta\partial t}+v_x\frac{\partial^2 w}{\partial\theta\partial x}\right)\right)\right.\\
&\left.+h_f\frac{\partial}{\partial x}\left(\mu\left(\frac{\partial^2 w}{\partial x\,\partial t}+v_x\frac{\partial^2 w}{\partial x^2}\right)\right)\right]+F_0\delta(x-x_m)\\
&=I_0\frac{\partial^2 w}{\partial t^2}-\left(\frac{4}{3h^2}\right)^2 I_6\left(\frac{\partial^4 w}{\partial x^2\partial t^2}+\frac{\partial^4 w}{R^2\partial\theta^2\partial t^2}\right)\\
&+\frac{4}{3h^2}\left(I_3\frac{\partial^3 u}{\partial t^2\partial x}+I_3\frac{\partial^3 v}{R\partial t^2\partial\theta}+J_4\left(\frac{\partial^3\psi_x}{\partial t^2\partial x}+\frac{\partial^3\psi_\theta}{R\partial t^2\partial\theta}\right)\right),
\end{aligned}
\tag{A3}
$$

$$
\begin{aligned}
&\delta\psi_x : B_{11}\left(\frac{\partial^2 u}{\partial x^2}+\frac{\partial w}{\partial x}\frac{\partial^2 w}{\partial x^2}\right)+B_{12}\left(\frac{\partial^2 v}{R\partial\theta\partial x}+\frac{\partial w}{R\partial x}+\frac{\partial w}{R\partial\theta}\frac{\partial^2 w}{R\partial\theta\partial x}\right)\\
&+D_{11}\left(\frac{\partial^2\psi_x}{\partial x^2}\right)+D_{12}\left(\frac{\partial^2\psi_\theta}{R\partial\theta\partial x}\right)+F_{11}\left(\frac{-4}{3h^2}\left(\frac{\partial^2\psi_x}{\partial x^2}+\frac{\partial^3 w}{\partial x^3}\right)\right)\\
&+F_{12}\left(\frac{-4}{3h^2}\left(\frac{\partial^2\psi_\theta}{R\partial\theta\partial x}+\frac{\partial^3 w}{R^2\partial x\,\partial\theta^2}\right)\right)\\
&+B_{66}\left(\frac{\partial^2 u}{R^2\partial\theta^2}+\frac{\partial^2 v}{R\partial\theta\partial x}+\frac{\partial^2 v}{R\partial\theta\partial x}\frac{\partial w}{R\partial\theta}+\frac{\partial w}{\partial x}\frac{\partial^2 w}{R^2\partial\theta^2}\right)\\
&+D_{66}\left(\frac{\partial^2\psi_x}{R^2\partial\theta^2}+\frac{\partial^2\psi_\theta}{R\partial\theta\partial x}\right)+F_{66}\left(\frac{-4}{3h^2}\left(\frac{\partial^2\psi_\theta}{R\partial\theta\partial x}+\frac{\partial^2\psi_x}{R^2\partial\theta^2}+2\frac{\partial^4 w}{R^2\partial x\,\partial\theta^2}\right)\right)\\
&-A_{44}\left(\frac{\partial w}{\partial x}+\psi_x\right)-D_{44}\left(\frac{-4}{h^2}\left(\psi_x+\frac{\partial w}{\partial x}\right)\right)+\frac{4}{h^2}\left(\begin{array}{l}D_{44}\left(\dfrac{\partial w}{\partial x}+\psi_x\right)\\ +F_{44}\left(\dfrac{-4}{h^2}\left(\psi_x+\dfrac{\partial w}{\partial x}\right)\right)\end{array}\right)\\
&+E_{11}\left(\frac{\partial^2 u}{\partial x^2}+\frac{\partial w}{\partial x}\frac{\partial^2 w}{\partial x^2}\right)+E_{12}\left(\frac{\partial^2 v}{R\partial x\,\partial\theta}+\frac{\partial w}{R\partial x}+\frac{\partial w}{R\partial\theta}\frac{\partial^2 w}{R\partial\theta\partial x}\right)\\
&+F_{11}\left(\frac{\partial^2\psi_x}{\partial x^2}\right)+F_{12}\left(\frac{\partial^2\psi_\theta}{R\partial\theta\partial x}\right)+H_{11}\left(\frac{-4}{3h^2}\left(\frac{\partial^2\psi_x}{\partial x^2}+\frac{\partial^3 w}{\partial x^3}\right)\right)\\
&+H_{12}\left(\frac{-4}{3h^2}\left(\frac{\partial^2\psi_\theta}{R\partial\theta\partial x}+\frac{\partial^3 w}{R^2\partial x\,\partial\theta^2}\right)\right)\\
&-\frac{4}{3h^2}\left(E_{66}\left(\frac{\partial^2 u}{R^2\partial\theta^2}+\frac{\partial^2 v}{R\partial x\,\partial\theta}+\frac{\partial^2 w}{R\partial x\,\partial\theta}\frac{\partial w}{R\partial\theta}+\frac{\partial w}{\partial x}\frac{\partial^2 w}{R^2\partial\theta^2}\right)\right.\\
&\left.+F_{66}\left(\frac{\partial^2\psi_x}{R^2\partial\theta^2}+\frac{\partial^2\psi_\theta}{R\partial x\,\partial\theta}\right)+H_{66}\left(\frac{-4}{3h^2}\left(\frac{\partial^2\psi_\theta}{R\partial x\,\partial\theta}+\frac{\partial^2\psi_x}{R^2\partial\theta^2}+2\frac{\partial^3 w}{R^2\partial x\,\partial\theta^2}\right)\right)\right)\\
&=J_1\frac{\partial^2 u}{\partial t^2}+K_2\frac{\partial^2\psi_x}{\partial t^2}-\frac{4}{3h^2}J_4\frac{\partial^3 w}{\partial t^2\partial x},
\end{aligned}
\tag{A4}
$$

$$
\begin{aligned}
&\delta\psi_\theta : B_{66}\left(\frac{\partial^2 u}{R\partial\theta\partial x}+\frac{\partial^2 v}{\partial x^2}+\frac{\partial^2 w}{\partial x^2}\frac{\partial w}{R\partial\theta}+\frac{\partial w}{\partial x}\frac{\partial^2 w}{R\partial\theta\partial x}\right)\\
&+D_{66}\left(\frac{\partial^2\psi_x}{R\partial\theta\partial x}+\frac{\partial^2\psi_\theta}{\partial x^2}\right)+F_{66}\left(\frac{-4}{3h^2}\left(\frac{\partial^2\psi_\theta}{\partial x^2}+\frac{\partial^2\psi_x}{R\partial\theta\partial x}+2\frac{\partial^3 w}{R\partial x^2\partial\theta}\right)\right)\\
&+B_{12}\left(\frac{\partial^2 u}{R\partial\theta\partial x}+\frac{\partial w}{\partial x}\frac{\partial^2 w}{R\partial\theta\partial x}\right)+B_{22}\left(\frac{\partial^2 v}{R^2\partial\theta^2}+\frac{\partial^2 w}{R^2\partial\theta}+\frac{\partial w}{R\partial\theta}\frac{\partial^2 w}{R^2\partial\theta^2}\right)\\
&+D_{12}\left(\frac{\partial^2\psi_x}{R\partial\theta\partial x}\right)+D_{22}\left(\frac{\partial^2\psi_\theta}{R^2\partial\theta^2}\right)+F_{12}\left(\frac{-4}{3h^2}\left(\frac{\partial^2\psi_x}{R\partial\theta\partial x}+\frac{\partial^3 w}{R\partial\theta\partial x^2}\right)\right)\\
&+F_{22}\left(\frac{-4}{3h^2}\left(\frac{\partial^2\psi_\theta}{R^2\partial\theta^2}+\frac{\partial^3 w}{R^3\partial\theta^3}\right)\right)-A_{55}\left(\frac{\partial w}{R\partial\theta}+\psi_\theta\right)\\
&-D_{55}\left(\frac{-4}{h^2}\left(\psi_\theta+\frac{\partial w}{R\partial\theta}\right)\right)+\frac{4}{h^2}\left(\begin{array}{l}D_{55}\left(\dfrac{\partial w}{R\partial\theta}+\psi_\theta\right)\\ +F_{55}\left(\dfrac{-4}{h^2}\left(\psi_\theta+\dfrac{\partial w}{R\partial\theta}\right)\right)\end{array}\right)\\
&-\frac{4}{3h^2}\left[E_{66}\left(\frac{\partial^2 u}{R\partial\theta\partial x}+\frac{\partial^2 v}{\partial x^2}+\frac{\partial^2 w}{\partial x^2}\frac{\partial w}{R\partial\theta}+\frac{\partial w}{\partial x}\frac{\partial^2 w}{R\partial\theta\partial x}\right)\right.\\
&+F_{66}\left(\frac{\partial^2\psi_x}{R\partial\theta\partial x}+\frac{\partial^2\psi_\theta}{\partial x^2}\right)+H_{66}\left(\frac{-4}{3h^2}\left(\frac{\partial^2\psi_\theta}{\partial x^2}+\frac{\partial^2\psi_x}{R\partial\theta\partial x}+2\frac{\partial^3 w}{R\partial x^2\partial\theta}\right)\right)\\
&+E_{12}\left(\frac{\partial^2 u}{R\partial\theta\partial x}+\frac{\partial w}{\partial x}\frac{\partial^2 w}{R\partial\theta\partial x}\right)+E_{22}\left(\frac{\partial^2 v}{R^2\partial\theta^2}+\frac{\partial^2 v}{R^2\partial\theta}+\frac{\partial w}{R\partial\theta}\frac{\partial^2 w}{R^2\partial\theta^2}\right)\\
&+F_{12}\left(\frac{\partial^2\psi_x}{R\partial\theta\partial x}\right)+F_{22}\left(\frac{\partial^2\psi_\theta}{R^2\partial\theta^2}\right)+H_{12}\left(\frac{-4}{3h^2}\left(\frac{\partial^2\psi_x}{R\partial\theta\partial x}+\frac{\partial^3 w}{R\partial\theta\partial x^2}\right)\right)\\
&\left.+H_{22}\left(\frac{-4}{3h^2}\left(\frac{\partial^2\psi_\theta}{R^2\partial\theta^2}+\frac{\partial^3 w}{R^3\partial\theta^3}\right)\right)\right]=J_1\frac{\partial^2 v}{\partial t^2}+K_2\frac{\partial^2\psi_\theta}{\partial t^2}-\frac{4}{3h^2}J_4\frac{\partial^3 w}{R\partial t^2\partial\theta},
\end{aligned}
\tag{A5}
$$